Moure, M.M., Feito, N., Aranda-Ruiz, J., Loya, J.A. y Rodríguez-Millán, M. (2019). On the characterization and modelling of high-performance para-aramid fabrics, *Composite Structures*, 212, pp. 326-337.

DOI: https://doi.org/10.1016/j.compstruct.2019.01.049

Funding: Ministry of Economy and Competitiveness of Spain under the Project RTC-2015-3887-8 and DPI2017-88166-R

On the characterization and modelling of high-performance para-aramid fabrics

M.M. Moure[a,*], N. Feito[b], J. Aranda-Ruiz[c], J.A. Loya[c], M. Rodriguez-Millan[b]

[a] University Carlos III of Madrid, Department of Bioengineering and Aerospace Engineering, Avda. Universidad 30, 28911Leganés, Madrid, Spain [b] University Carlos III of Madrid, Department of Mechanical Engineering, Avda. Universidad 30, 28911Leganés, Madrid, Spain [c] University Carlos III of Madrid, Department of Continuum Mechanics and Structural Analysis, Avda. Universidad 30, 28911Leganés, Madrid, Spain

A B S T R A C T

In this work, seven different types of fabrics based on para-aramid yarns with different interlacing geometries and reinforcement polymer matrix have been characterised and compared from yarn level to weave level. Mechanical properties such as maximum stress, failure strain, and elastic modulus have been obtained from uniaxial tensile tests, while the inter-yarn friction coefficients (s tatic an d ki netic) ha ve be en ob tained by a combination of single yarn pull-out tests and an analytical model. Results show that mechanical properties are quite similar at yarn level but different at fabric level. Thus, the geometry, orientation and section of the yarn play an important role in the mechanical properties of the fabric. As an application of these results, a mesoscopic three-dimensional numerical model has been developed, and simulations of ballistic impact test have been carried out validating the model with experimental tests.

Keywords:
Fabric
Aramid fibre
Yarn pull-out
Mechanical testing
Impact
Numerical model

1. Introduction

High-performance fabrics manufactured in aramid have increased their demand in recent years in applications where high levels of energy absorption are required, as is the case of structures and personal protections under impact loadings. This increase has been mainly driven by their desired engineering properties, such as high elastic modulus, high strength, low density, good chemical resistance and thermal stability [1]. Most of the fabrics used in the design of personal protections and structures under impact loadings are plain woven fabrics, in which yarns are interlaced in two orthogonal directions. The fill yarn passes alternately above and below each yarn or set of yarns in which the warp is divided. Aramid yarns and interlacing geometries have been developed and optimised according to their use in different applications.

The sliding between yarns inside fabric plays an important role in the in-plane mechanical response of the material, leading to a large-scale deformation of the yarns. This deformation process is responsible for the energy absorption of the fabric and the loss of orthogonality in the main directions of the material [2]. The slippage of the yarn also influences the stress concentration near the damaged region of the fabric and in the damage propagation [3]. Tapie et al. [4] revealed that the influence of the weaving in the mechanical response of the yarns is of great importance; crimp yarns possess higher strength and stiffness, but a lower failure strain, compared to neat yarns.

Friction between yarns plays an important role in response to the impact of aramid fabrics, both in a direct and indirect way. The direct effect is reflected in an increase of the energy dissipation of the fabric when the yarns begin to move one concerning the other, either through sliding, stretching or reorienting the yarn. The indirect effect i s reflected in the way the loads are transferred and redistributed between neighbour yarns [5]. Also, other studies have numerically analysed and compared the influence of the friction between fabric and projectile, and between the yarns during an impact [6], concluding that the latter interaction is the one that plays the most important role in the response of the fabric to impact.

One of the most used experimental techniques to study the inter-yarn friction is the yarn pull-out test [1,2,5,7–19]. From these experimental works, the authors concluded that the maximum pull-out force is greater for warp than for fill yarns [5,18]. This is attributed to the larger crimp in the warp yarns of an un-tensioned fabric compared to the fill y arns. I n b oth d irections, t his f orce i ncreases proportionately with the length of the specimen and with the applied preload [14,15,18] and decreases with the pull-out speed [5]. Also, Dong and Sun [1] established that in an impact test, energy dissipation during perforation increases with maximum pull-out force. Summarizing, the yarn pull-out forces depend on fabric areal density, fabric sample dimensions and number of pulled ends in the fabric, and it is also higher in fabrics with high density [8].

Despite the substantial number of works that carry out pull-out tests, the number of experimental papers that estimate the value of the friction coefficient is not enough. Generally, the authors have obtained the friction coefficient in a type of fabric, unlike the study carried out in this paper, in which a comparison between seven different fabrics is made. Rao et al. [20] carried out quasi-static experiments to obtain the friction coefficient and incorporated it into impact models. The main conclusion showed that while friction improves ballistic performance by maintaining the integrity of the weave pattern, material properties of the yarns have a significant influence on the effect of friction. It would be worth mentioning the study carried out by Das et al. [13], in which an analytical model is presented, used to determinate the static and dynamic friction coefficients from the pull-out force vs displacement curve obtained from a yarn pull-out test.

Regarding the characterization of the fabric, there are not many studies in which tensile test are carried out. This is mainly because most of the studies include numerical models at mesoscale and not at macroscale. Mesoscale studies are interesting to carry out the analysis of a simple fabric; however, when you want to carry out the study of a bulletproof vest made up with a large number of layers, it is convenient to use macro-scale models due to the high computational cost. Sretis et al. [21] focused on the mechanical response of para-aramid protection fabrics under tensile loading. The experimental results indicated that knitting angle affects both the fracture propagation mode and the fracture toughness. Finally, Beex et al. [22] carried out experiments in in-plane directions (warp and fill) to implement a numerical model for woven materials which consists of a network of trusses, which represent the response of the yarns.

A useful tool to better understand the behaviour of aramid materials under impact loads is the use of numerical models. The ballistic limit (known as V_{50}), the deformation shape of the woven or the influence of the inter-yarn friction can be studied using the Finite Element Method. A study of the characterization of the yarns is useful to implement mesoscopic models from which to study the parameters mentioned previously [20,23–28].

The main objective of the present work is to compare the mechanical behaviour and the intern-yarn friction coefficients in seven different types of aramid fabrics (different areal densities and reinforcements) in quasi-static conditions. Therefore, an intensive test campaign based on uniaxial tensile tests and yarn pull-out tests has been developed to obtain the necessary properties for the development of future studies and numerical models based on Finite Elements Analysis. With the properties estimated in this work for para-aramid fabrics, a ballistic impact model has been developed and validated with experimental tests.

2. Experimental program

2.1. Materials

For the development of this work, a total of seven woven aramid fabrics with different areal densities are analysed (Table 1 and Fig. 1). All these fabrics are made of aramid Kevlar®K129, supplied by HONEYWELL, a common para-aramid used in vest protections due to its excellent properties for impact energy absorption.

The first four types of plain-woven fabrics shown in Table 1 and Fig. 1 (from A to D) have the same interlacing geometry, but different yarns width, and do not present any polymer reinforcement; from now on they will be named *"soft fabrics"* in this study. Relevant dimensions related with the geometry both in warp and fill directions were mea-sured by microscopy (as shown in Fig. 2a) and are resumed in Table 2; where w is the width of the yarn section, λ is the span length, h is the thickness of the yarn, δ is the vertical distance between the neutral axis (center line) of two adjacent crests of the yarn, δ_0 is the vertical distance between the vertical projections of the previous point on the interface of warp and fill yarns and θ is the warp angle (as it is specified in Fig. 2b). Also, the yarn density of each type of fabric is included in Table 2.

Table 1
Areal density and thickness of the plain-woven fabrics analysed. From A to D (*soft fabrics*) and from E to G (*hard fabrics*).

Fabric	*Type of Fabric*	*Areal density* (g/m^2)	*Thickness* (mm)
A	*Soft Fabrics*	204.100	0.3506
B		211.450	0.3650
C		114.590	0.2180
D		124.450	0.1970
E	*Hard Fabrics*	310.000	0.2500
F		301.237	0.2250
G		108.363	0.1100

The next three materials, shown in Table 1 and Fig. 1 (from E to G), are reinforced with resin, and they will be named "*hard fabrics*" in this study. These fabrics are made of one layer of interlacing aramid yarns coupled in both sides with a thermoplastic film. The last material (G) consists of two plies of unidirectional aramid fibre cross-plied at 0°/90°.

2.2. Test set-up

In this section, the methodology carried out to characterise the different types of fabrics is presented. Experimental uniaxial tensile tests on yarns and weaves of soft and hard fabrics, and also yarn pull-out tests on soft fabrics, are performed to obtain the most important mechanical properties and the inter-yarn friction coefficients.

2.2.1. Yarn uniaxial tensile tests

To understand the deformation process of a fabric armour system during impact, the behaviour of their single constituent fibre needs to be examined first. A detailed description of the mechanical properties of single fibres is necessary to understand the yarn mechanics. To carry out this first set of experiments, yarns from the four soft fabrics (A to D) are extracted carefully from the weave to ensure that the filaments did not suffer any damage. Elastic modulus (E), maximum stress (σ_{max}), maximum strain (ε_{max}) and energy absorbed per unit volume (E_v) in the longitudinal direction of the yarns are obtained by uniaxial tensile tests in both directions (fill and warp). The energy density (energy absorbed per unit volume) is estimated as the area under the stress–strain curve (Eq. (1)),

$$E_V = \int_0^{\varepsilon_f} \sigma \, d\varepsilon \tag{1}$$

All tests are conducted on an INSTRON 8516 universal testing machine with a 5 kN load cell and a velocity of 10 mm/min. To guarantee the results repeatability, five tests were done for each direction, as can be seen in the stress–strain curves of Fig. 3b. Specimens were rolled around a wood rod and glued to minimize slippage, then held in position by metallic grips as recommended in the standard of UNE-EN ISO 2062 [29].

2.2.2. Yarn pull-out tests

Experimental works from the literature showed that friction between yarns affects the ballistic impact energy absorption of these fabrics [18,30,31].

The experiment consists of extracting an individual yarn from the middle width of a fabric specimen (size $w \times L_0$) (120 mm × 50 mm) (see Fig. 4a). The fabric is attached to a U-shaped clamping frame where fill and warp yarns are well aligned with the frame with no pretension. Clamps were used to apply the required pressure to both edges of the fabric sample via the U shape so that all fill yarns have limited movement at their ends, allowing the pulling-out yarn to slide through them. The U Shape is fixed to the bottom grip of the tensile testing

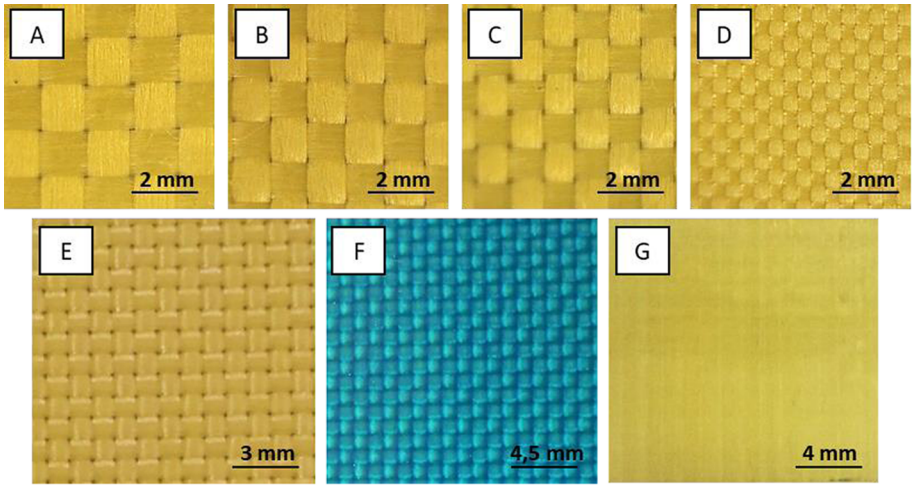

Fig. 1. Microscopic pictures of the fabrics analysed (view in the plant). A–D (*soft fabrics*) and E–G (*hard fabrics*).

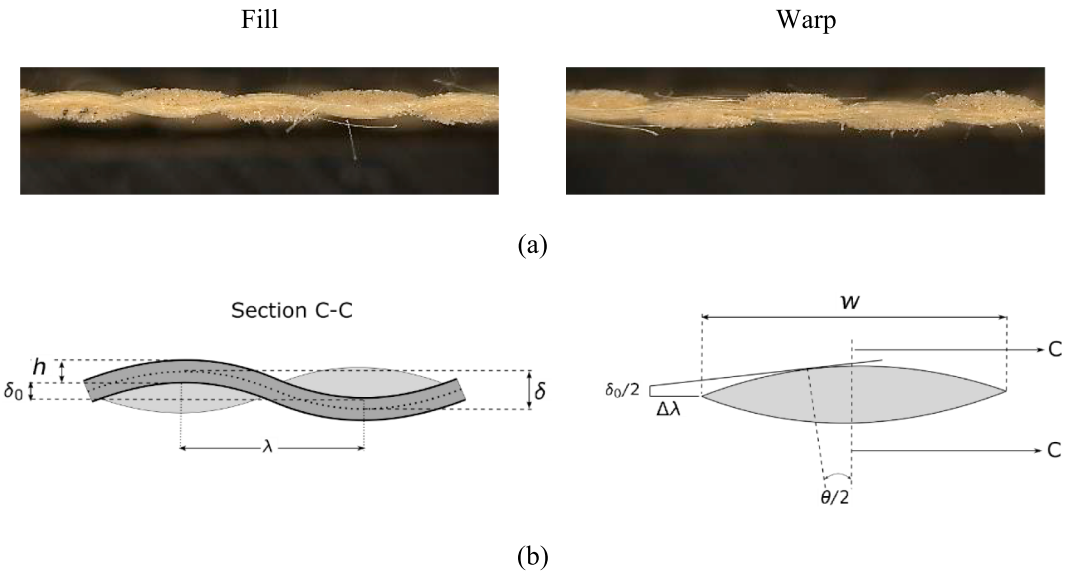

Fig. 2. (a) Fill cross section (left) and warp (right) measured by microscopy (representative picture). (b) Outline of the geometry of a yarn with the most relevant dimensions.

Table 2
Relevant dimensions of the yarns for *soft fabrics*.

Fabric-Yarn orientation	*Yarn density* (threads/cm)	*w* (mm)	*h* (mm)	λ (mm)	*Cross Yarn Section* (mm^2)	*δ* (mm)	δ_o (mm)	*θ/2* (°)
A-Fill	8.5 ± 0.3	1.1420	0.1753	1.1520	0.0647	0.1650	0.0610	5.22
B-Fill	10.7 ± 0.3	0.8985	0.1825	0.9545	0.0549	0.1510	0.0400	9.81
C-Fill	12.2 ± 0.3	0.6760	0.1090	0.8476	0.0278	0.0810	0.0170	7.62
D-Fill	27.5 ± 0.3	0.3520	0.0985	0.3970	0.0117	0.1310	0.0470	11.73
A-Warp	8.5 ± 0.3	1.0950	0.1753	1.1650	0.0687	0.1760	0.0773	6.43
B-Warp	10.7 ± 0.3	0.9050	0.1825	0.9305	0.0527	0.1830	0.0473	10.30
C-Warp	12.2 ± 0.3	0.7473	0.1090	0.8563	0.0238	0.1153	0.0265	9.35
D-Warp	27.5 ± 0.3	0.3600	0.0985	0.3636	0.0120	0.0895	0.0304	7.80

machine (INSTRON 8516). The other grip holds on to the top end of the innermost warp yarn rolled around a wood rod and glued to minimize slippage. The yarn is pulled out at a speed of 5 mm/s in the vertical direction. Each fabric type is tested five times to guarantee the repeatability of the procedure.

As depicted in Fig. 4a, L_0 = 50 mm and l_o = 10 mm are the lengths of the part of the longitudinal yarn embedded in the fabric and the tail length (part kept unconstrained at the rear end) respectively. To avoid any shear displacement before the yarn pull out test, the fabric was positioned completely horizonal respect to the frame without applying any pretension, and therefore any shear displacement.

A typical pull-out force–displacement curve is obtained from the yarn pull-out test as shown in Fig. 4b. Initially, the fabric experiences a deformation in the plane itself without any relative displacement between yarns, being the necessary force to achieve this status P_{in} (see Fig. 4a). Once P_{in} force value is reached, three different zones are defined. A first region (region I), also referred to as the loading region, where the uncrimp (loss of the wavy shape of the yarn) and stretching

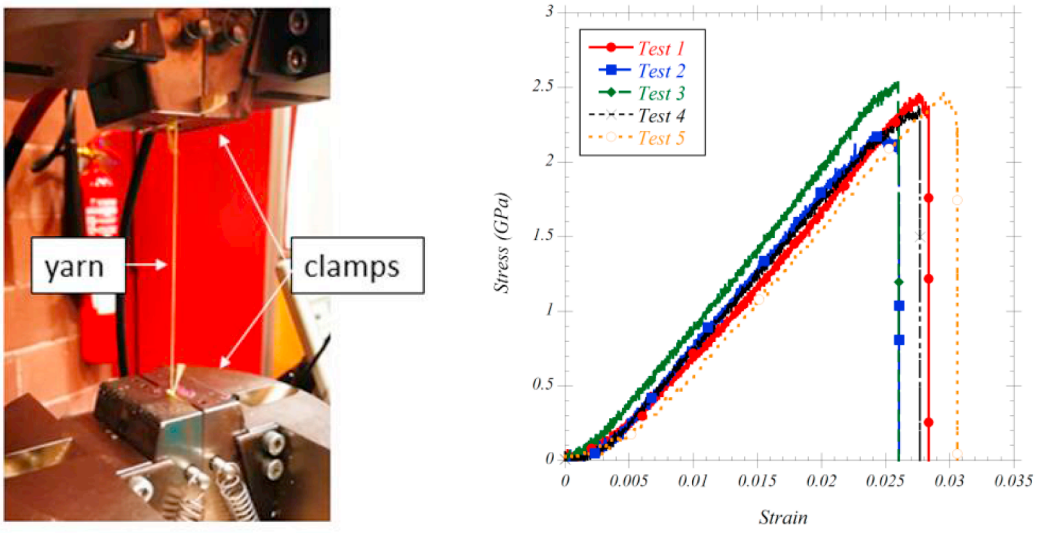

Fig. 3. (a) Uniaxial tensile test device. (b) Test results example for fabric A in fill direction.

of the yarn occurs, resulting in an out-of-plane displacement (total uncrimp ΔL in Fig. 4b). The boundary value established by the border of this region corresponds to the maximum value of the pull-out force, called P_{static} since the nature of the strength in this region is purely static. Region II encompasses a transition zone in which the relative displacement of the yarn from which it is pulled concerning the transverse yarn begins, in which the nature of the movement goes from static to kinetic. After this transition zone, a constant pull-out force value is set until the end of the extracted yarn reaches the contact area with the transverse yarn on the lower edge of the specimen, referred to as tail length ($l_0 = 10$ mm) in Fig. 4b. The boundary value set by the border of this region corresponds to the value named $P_{kinetic}$, since this zone is dominated by kinetic friction. Finally, in region III, it is produced a progressive descent of the pull-out force as the effective number of cross-yarns decreases.

The methodology used to calculate the inter-yarn friction coefficient follow the Euleŕs belt friction formulas, Eqs. (2) and (3), described in detail in [13]. Yarn pull-out tests are needed to calculate different parameters of the equations,

$$\frac{P_{static}}{(P_{in}/n)} = e^{n\cdot\mu_S\cdot\theta} \rightarrow \mu_S = \frac{Ln\left[\frac{P_{static}}{(P_{in}/n)}\right]}{n\cdot\theta} \tag{2}$$

$$\frac{P_{kinetic}}{(P_{in}/n)} = e^{n\cdot\mu_k\cdot\theta} \rightarrow \mu_k = \frac{Ln\left[\frac{P_{kinetic}}{(P_{in}/n)}\right]}{n\cdot\theta} \tag{3}$$

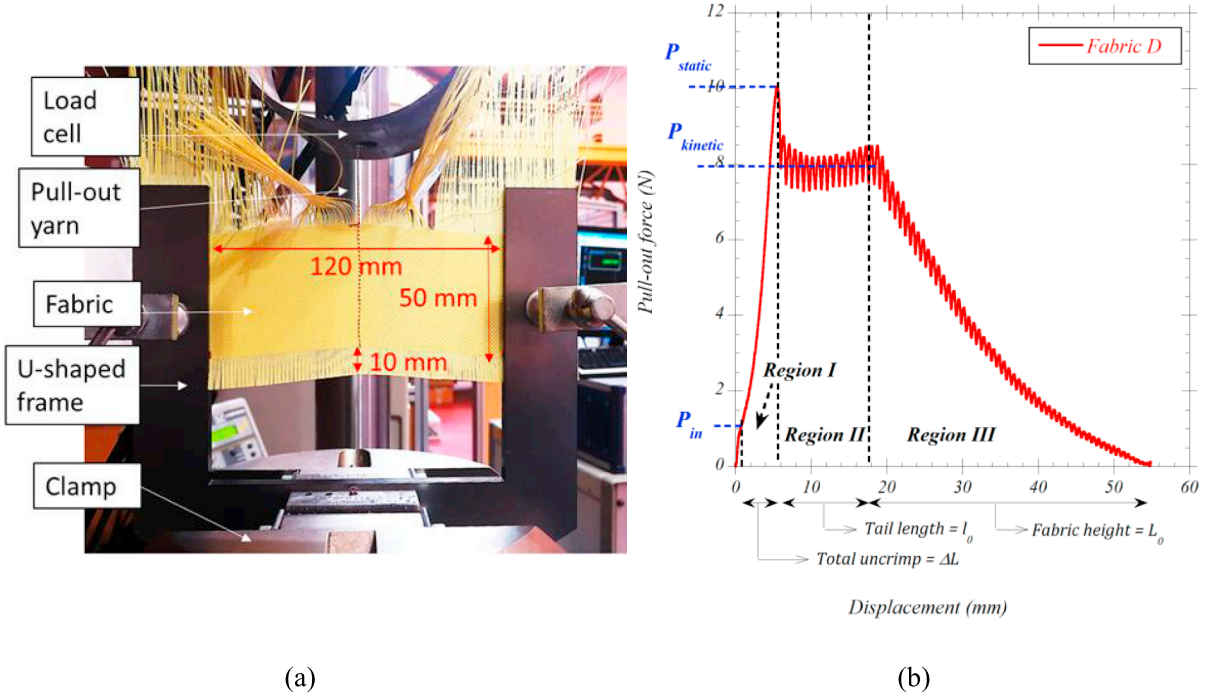

Fig. 4. (a) Yarn pull-out test set-up. (b) Typical force–displacement curve of a yarn pull-out test.

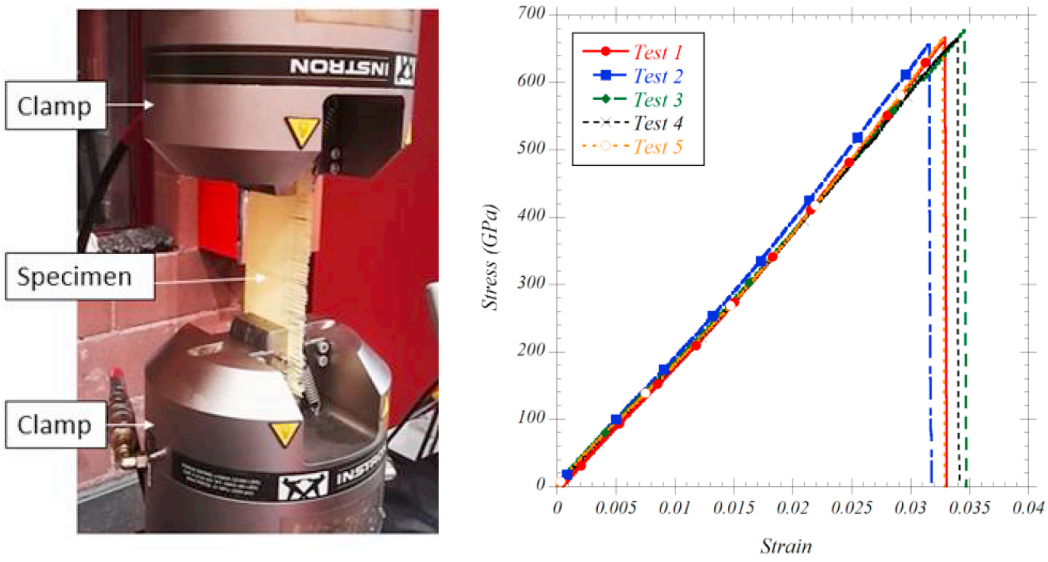

(a) (b)

Fig. 5. (a) Set-up for the fabric tensile test. (b) Example of the five tests carried out for fabric F.

where n is the number of cross over yarns (determined as $n = L_0/s + 1$, where s is the yarn span), μ_S and μ_k are the static and kinetic friction coefficients respectively; and θ is the warp angle, determined as specified in [13].

2.2.3. Fabric uniaxial tensile tests

Uniaxial tensile tests at 5 mm/min were performed on fabric specimens in fill and warp directions, as mentioned in Section 3.1.

Fig. 5a. shows the experimental set-up, being the effective area of the fabric 30 × 110 mm^2. The tensile specimen is mounted between the upper and lower grips. Rubber squares were sandwiched between the grips to avoid slippage as recommend the standard UNE-EN ISO 13934-1 [32]. Five tests were repeated in each direction to ensure the repeatability of the procedure. Fig. 5b shows the tests of fabric F as a representative case.

From the stress–strain curves, the mechanical properties in fill and warp directions for soft fabrics and hard fabrics are obtained, and are shown in the following section.

3. Results and discussion

3.1. Yarn uniaxial tensile tests

Fig. 6 shows one example of the stress–strain curves for each soft fabric (A to D) for both fill and warp yarns. From the stress–strain curves, the mechanical properties of each soft fabric in both directions

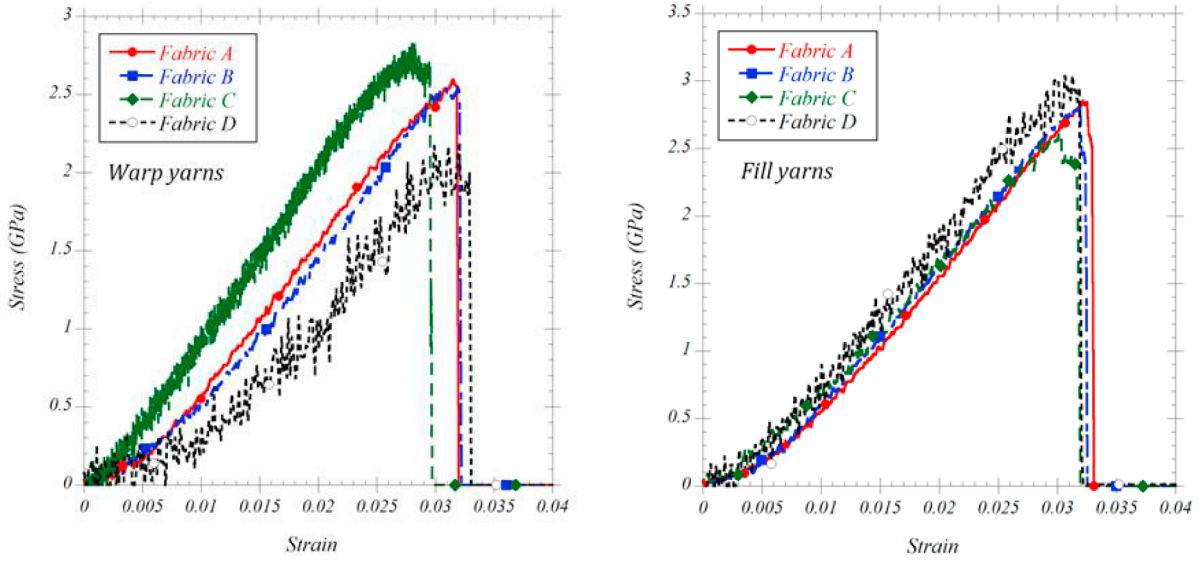

(a) (b)

Fig. 6. Examples of stress–strain curves for all soft fabrics in (a) warp yarns and (b) fill yarns.

Table 3
Mechanical properties of fill and warp yarns for soft fabrics.

Fabric-Yarn orientation	F (N)	E (GPa)	σ_{max} (GPa)	ε_{max}	E_V (MJ/m^3)
A-Fill	158.612 ± 14.249	101.740 ± 2.596	2.451 ± 0.220	0.029 ± 0.001	35.5 ± 4.6
B-Fill	140.036 ± 9.237	103.205 ± 1.669	2.549 ± 0.168	0.029 ± 0.001	36.9 ± 3.8
C-Fill	65.516 ± 1.701	93.408 ± 1.662	2.934 ± 0.061	0.029 ± 0.001	42.5 ± 2.4
D-Fill	33.937 ± 1.072	114.678 ± 2.599	2.892 ± 0.091	0.029 ± 0.001	41.9 ± 2.8
A-Warp	166.065 ± 4.334	99.898 ± 1.868	2.416 ± 0.063	0.029 ± 0.002	35.0 ± 3.4
B-Warp	132.984 ± 0.092	106.126 ± 3.119	2.523 ± 0.002	0.029 ± 0.001	36.6 ± 1.3
C-Warp	69.943 ± 1.537	113.040 ± 2.354	2.355 ± 0.065	0.031 ± 0.001	36.5 ± 2.2
D-Warp	25.142 ± 0.313	96.402 ± 2.981	2.092 ± 0.023	0.033 ± 0.001	34.5 ± 1.5

are obtained. Table 3 summarises the most relevant properties of each yarn: the elastic modulus (E), maximum force (F_{max}), failure stress (σ_{max}), failure strain (ε_{max}) and absorbed energy density (E_V).

Slight differences between yarn orientations are found according to the results shown in Table 3. The maximum stresses are higher in the case of fill yarns; however, the failure strains are quite similar in both directions. Therefore, the absorbed energy density is higher in the case of fill yarns. These results are in accordance with the findings of Das et al.[13] for a single tested fabric. It can be verified that the lower the areal density of the fabric, the greater the difference in the failure stress between the fill and warp directions. The maximum force that the yarn can support up to failure increases with the width of the yarn section, and therefore, the maximum force increases from fabric D to A.

3.2. Yarn pull-out tests

In Fig. 7, the pull-out force vs displacement curve of each fabric is presented. The maximum pull-out force increases with the number of transverse threads that the yarn pulled-out must cross. The number of transverse yarns to be crossed in each fabric is around 140 for fabric D, and between 44 and 60 for the remaining three (fabrics A to C); therefore, the maximum value of pull-out force is obtained for fabric D while for fabrics A to C the value is similar.

The inter-yarn friction coefficients has been obtained by means of the analytical model of Das et al. described in [13] (see Eqs. (2) and (3)). The static (μ_s) and kinetic (μ_k) friction coefficients

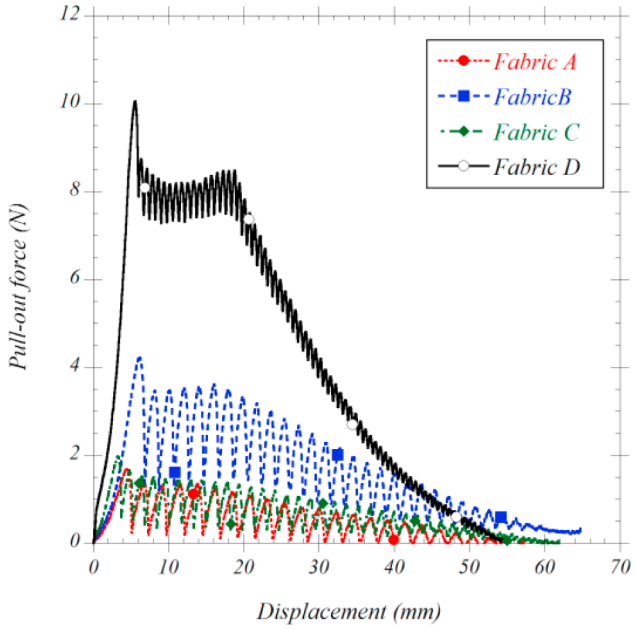

Fig. 7. Pull-out force–displacement curve for the four soft fabrics studied.

Table 4
Static (μ_s) and kinetic (μ_k) friction coefficients for each fabric in both directions.

Fabric-Yarn orientation	P_{in} (N)	P_{static} (N)	$P_{kinetic}$ (N)	μ_s	μ_k	$\mu s/\mu k$
A-Fill	1.23	7.85	5.64	0.63	0.54	1.17
B-Fill	0.22	1.81	0.91	0.34	0.31	1.10
C-Fill	0.30	3.36	1.80	0.40	0.35	1.14
D-Fill	0.15	1.50	0.65	0.12	0.11	1.09
A-Warp	0.90	11.73	8.54	0.62	0.53	1.17
B-Warp	0.18	1.94	0.82	0.34	0.30	1.13
C- Warp	0.32	3.68	1.90	0.33	0.29	1.14
D- Warp	0.16	1.65	0.70	0.23	0.22	1.05

obtained in each direction for the different fabrics are collected in Table 4.

In general, the value of the kinetic inter-yarn friction coefficient is slightly lower than the static coefficient, as indicated by the ratio $\mu s/\mu k$ (Table 4); and which is in accordance with the results obtained by Das et al. [13] in the only fabric they performed. Both static and kinetic coefficients increase with the yarn width, as shown in Fig. 8a and b for fill and warp directions respectively. This increase occurs because the contact surface between yarns during the pull-out process is greater the higher the width. Therefore, the values of the friction coefficients be-tween fabric B and C are very close as the yarn width is quite similar in both cases. Additionally, comparing the results for each fabric in both directions, it is observed that for fabrics from A to C the friction coef-ficients are slightly smaller in warp direction than fill direction, while for fabric D the values for warp direction are almost the double than for fill direction.

Moreover, it is observed that the maximum pull-out force (P_{static}) is greater for warp than for fill yarns, result consistent with the conclusions given in the literature [5,18].

3.3. Fabric uniaxial tensile tests

In this section, the results corresponding to uniaxial tensile tests carried out on the seven fabrics presented in Table 1 of Section 2 (soft and hard fabrics), are presented. With these test, the mechanical properties at weave level are obtained.

Figs. 9 and 10 show an example of the stress–strain curves of the fabrics analysed for both fill and warp directions. The mechanical behaviour of soft fabrics (A to D) can be assumed elastic up to failure (see Fig. 9) in agreement with other authors in the literature [16,18].

Regarding the shape of the stress–strain curves, they are similar for soft fabrics. In A-D fabrics, four distinct regions are observed: crimp region, linear pre-peak region, linear post-peak region and non-linear post-peak region [19], Fig. 9a. and b.

Some differences between the stress–strain curves in both directions are observed. Fabric D has a larger crimp region than the others. It should be noted that this region increases when the test is conducted in warp direction, Fig. 9b. This could be explained attending to the influence of the weft yarns density into the warp shrinkage. It was

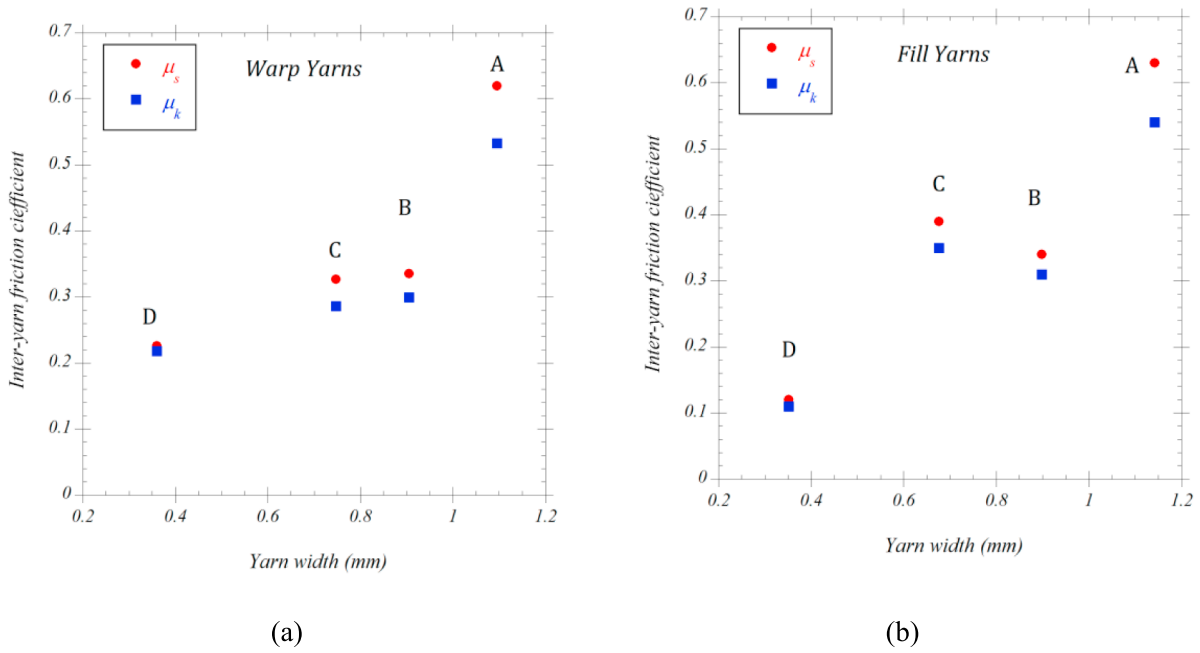

Fig. 8. Evolution of the static and dynamic inter-yarn friction coefficients with the yarn width. (a) Warp direction. (b) Fill direction.

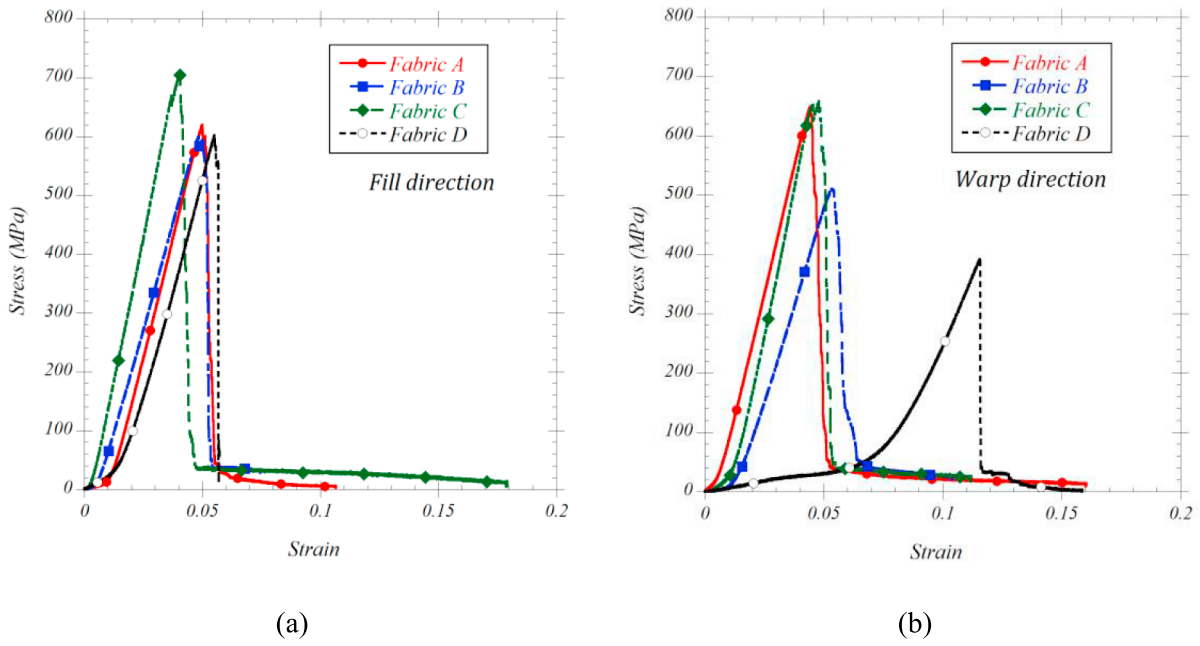

Fig. 9. Stress–strain curves for Soft fabrics (A–D): (a) Fill direction. (b) Warp direction.

reported in the literature that the higher value of the warp shrinkage, the bigger elongations on the weave [33]. Table 2 shows that the weft density of fabric D is higher than the double of the other three soft fabrics. It was also proved that yarn weave is more relevant in warp direction than in weft direction [22]. The maximum stress difference is approximately 200 MPa between both directions, for the case of fabric D.

In the case of hard fabrics, Fig. 10a and b, fabric G shows an almost linear behaviour up to breakage, while fabrics E and F show a non-linear behaviour until matrix cracking and its consequent yarn failure. This behaviour is particularly remarkable in the case of F fabric and may be due to its lower density and lower resin concentration. According to Bilisik et al. [34], three different regions can be identified in the stress–strain curves: first an inter fiber friction stage, where yarn to yarn friction and initial micro shear occurs. Second, a crimp stage occurs, where warp crimp decreases, and at the same time, probably fill crimp increases, and large fabric extension is obtained. Finally, the yarn extension stage occurs, where uncrimped yarn is almost entirely exhibited in the load extensions curve.

Fracture mode occurred within the gauge section is analysed in all cases. Breakage onset is associated with a sudden drop of the load; the failure is due to yarn pull-out and breakage of several yarns for soft fabrics, see Fig. 11a, c and e. However, in the case of hard fabrics, the fracture of the specimen is due to the matrix cracking and disheveled yarns as can be observed in Fig. 11b, d and f.

The failure mechanisms are related to damage concentration in a narrow area in the case of hard fabrics, with strong fibers deformation and breakage. The presence of a thermoplastic matrix, does not allow

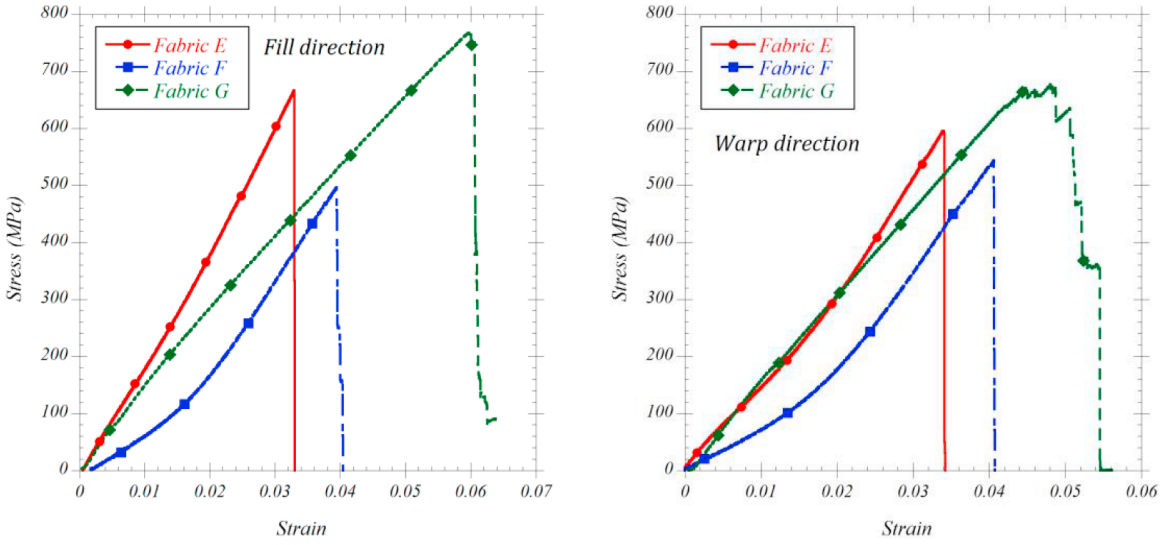

Fig. 10. Stress–strain curves for hard fabrics (E–G): (a) Fill direction. (b) Warp direction.

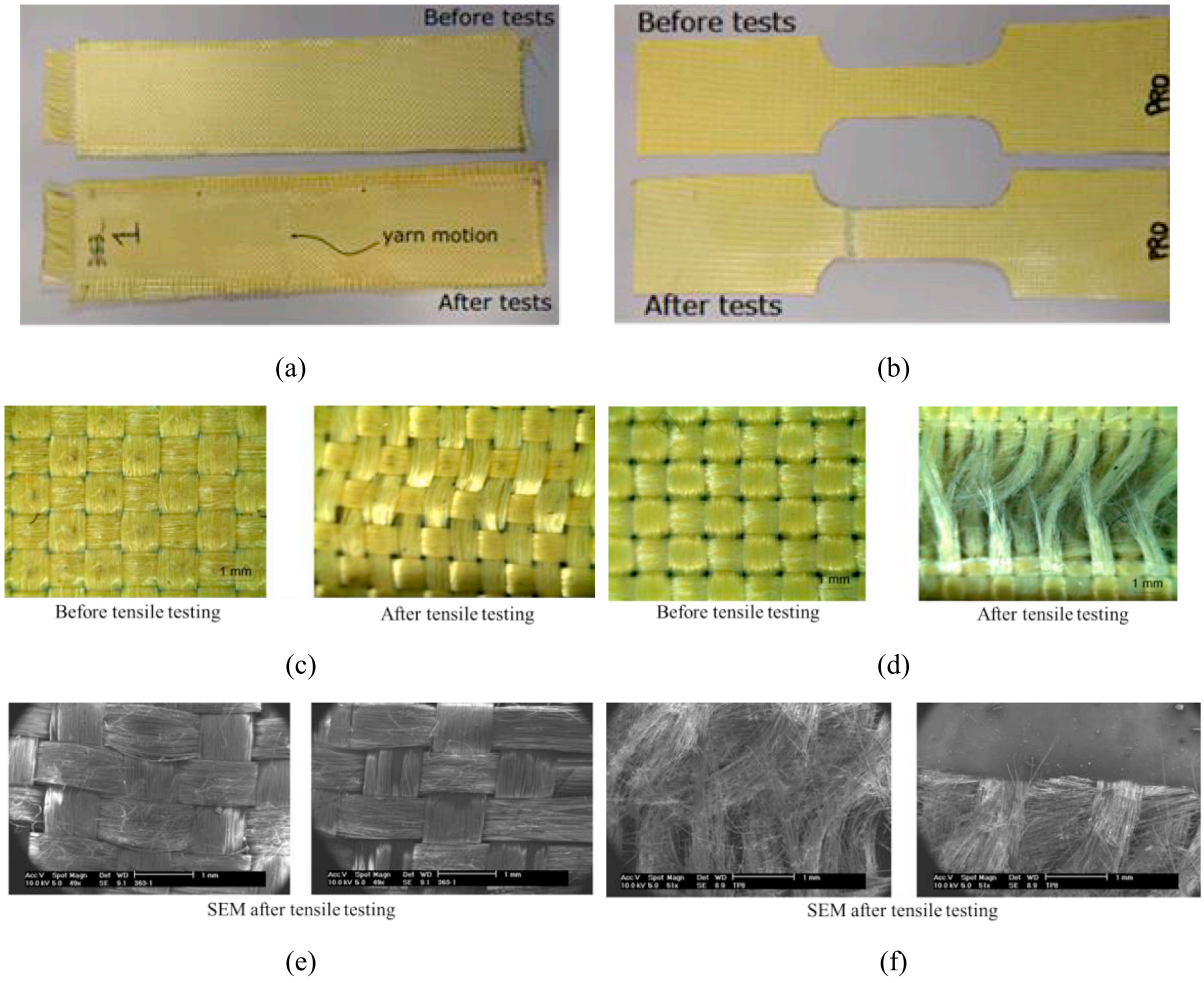

Fig. 11. Samples and fractured samples for (a) soft and (b) hard fabrics. Optical pictures for (c) soft and (d) hard fabrics. SEM pictures for (e) soft and (f) hard fabrics.

Table 5
Mechanical properties of one ply of the fabrics.

Fabric-Yarn orientation	E (GPa)	σ_{max} (MPa)	ε_{max}	E_V (MJ/m^3)
A-Fill	16.82 ± 0.082	632.25 ± 8.09	0.052 ± 0.001	16.33 ± 0.16
B-Fill	14.04 ± 0.157	596.18 ± 3.55	0.052 ± 0.001	15.58 ± 0.32
C-Fill	20.05 ± 0.093	681.54 ± 11.97	0.046 ± 0.001	15.75 ± 0.28
D-Fill	14.75 ± 0.207	580.31 ± 12.32	0.056 ± 0.001	11.92 ± 0.46
E-Fill	11.16 ± 0.514	513.62 ± 10.28	0.039 ± 0.001	10.17 ± 0.31
F-Fill	19.92 ± 0.206	666.52 ± 3.11	0.033 ± 0.001	11.11 ± 0.22
G-Fill	15.21 ± 0.977	753.03 ± 14.66	0.055 ± 0.002	20.88 ± 1.16
A-Warp	16.27 ± 0.196	602.43 ± 9.13	0.054 ± 0.002	16.98 ± 0.98
B-Warp	13.49 ± 0.225	515.75 ± 29.07	0.059 ± 0.002	15.48 ± 1.37
C-Warp	19.41 ± 0.124	668.70 ± 7.39	0.052 ± 0.001	17.46 ± 0.41
D-Warp	8.54 ± 0.157	396.77 ± 4.81	0.117 ± 0.001	12.53 ± 0.45
E-Warp	10.49 ± 0.122	515.02 ± 10.02	0.040 ± 0.001	10.42 ± 0.23
F-Warp	16.62 ± 0.135	576.05 ± 12.12	0.035 ± 0.001	9.95 ± 0.36
G-Warp	15.19 ± 0.857	765.62 ± 13.24	0.055 ± 0.002	21.05 ± 1.05

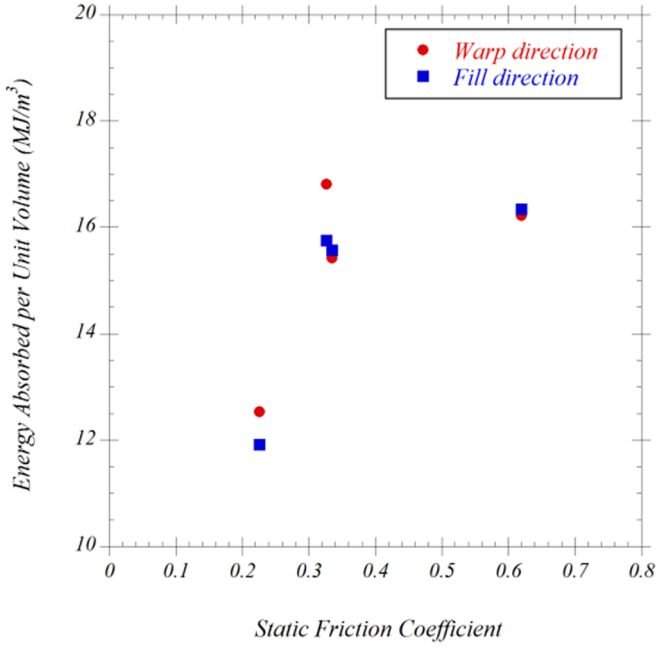

Fig. 12. Absorbed energy by the fabric as a function of the static friction coefficient.

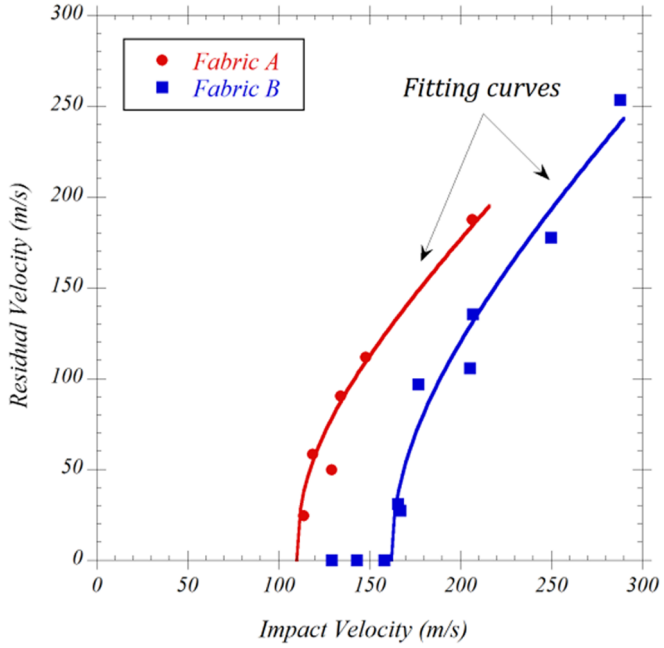

Fig. 14. Experimental residual velocity vs impact velocity curve for fabrics A and B.

the fibers located out of the failure zone to deform, being embedded in the rigid matrix. In the case of soft fabrics, the deformation occurs in the whole specimen leading to higher level of absorbed energy density. These observations indicate that soft fabrics may be good candidates for flexible protection development; however, because of the flexibility of soft fabrics, it cannot be solely considered for the design of this type of personal protection.

Table 5 summarises the most relevant properties of each fabric: elastic modulus (E), maximum force (F_{max}), maximum stress (σ_{max}), failure strain (ε_{max}) and absorbed energy density (E_V).

It has been found, that the fabric that absorbs the higher amount of energy density is the unidirectional fabric (G) followed by soft fabrics (A-D). This may be due to the fact that the behaviour of the fabric G is more similar to the soft fabrics than the hard fabrics because of the very

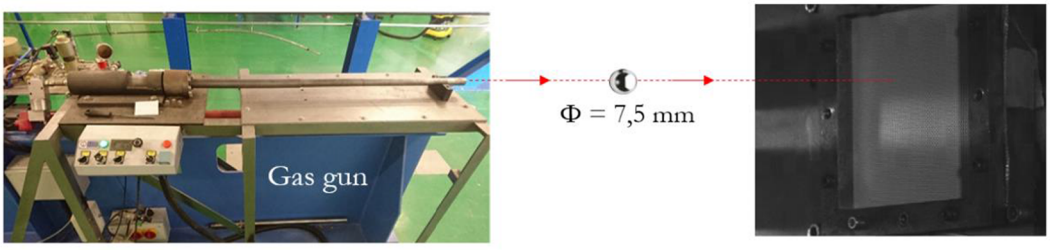

Fig. 13. Ballistic impact test set-up and fixation of the fabric in the frame.

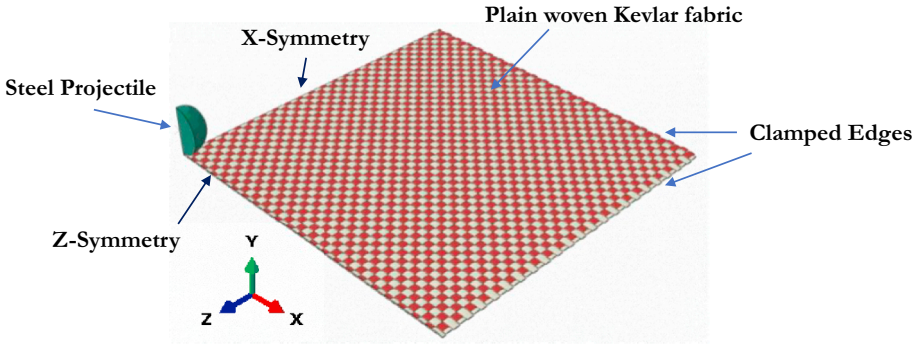

Fig. 15. Outline of the Finite Element Model designed.

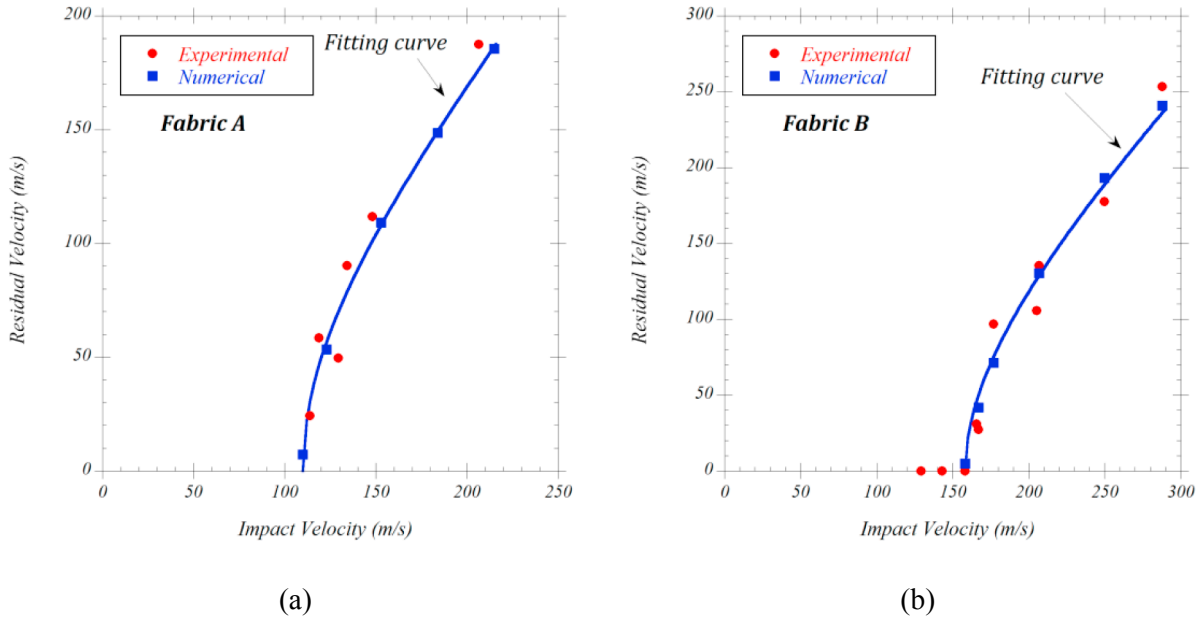

(a) (b)

Fig. 16. Experimental vs numerical results of the ballistic curve. (a) Fabric A. (b) Fabric B.

Table 6
Comparison between experimental and numerical results for impact tests on fabrics A and B.

	Fabric	*Ballistic limit* (m/s)	κ
Experimental	A	110	2.31
Numerical	A	110	2.05
Error (%)	A	0.00	11.25
Experimental	B	162	2.05
Numerical	B	158	1.92
Error (%)	B	2.47	6.34

small thickness of thermoplastic matrix (as can be seen in Table 1). Although the ballistic behaviour of fabrics is a complex problem which depends on numerous parameters, the energy density could be considered as one of the most relevant in order to analyze the impact behaviour of the fabric.

As mentioned and observed in Fig. 11c, there is a slipping of the yarn which ultimately leads to a decrease in the mechanical properties of the fabric. The yarn slippage occurs when the gradient in tension along a yarn is large enough to overcome the friction between the yarn and its crossing yarns [35]. The effect of the static friction coefficient on the energy absorbed per unit volume is illustrated in Fig. 12, resulting in an increase of the latter with the friction coefficient both in fill and warp directions.

4. Application of the mechanical properties to analyze the impact behaviour of aramid fabrics

As an application of the results obtained in Sections 2 and 3, a numerical ballistic impact model capable of reproducing experimental results has been developed (Section 4.2). For that purpose, among all the woven studied, fabrics A and B have been selected to perform the ballistic impact tests shown in Section 4.1.

4.1. Experimental results

Ballistic impact tests were carried out using a 7.62 mm caliber gas-gun to launch spherical aged martensitic steel projectiles of 7.5 mm diameter and 1.7 g mass (Fig. 13). The impacts were carried out on fabrics A and B with dimensions 100 × 100 mm^2 clamped on a steel frame as shown in Fig. 13 (right). The tests were carried out at room temperature (20 °C), using different impact velocities. Both the initial impact and the residual velocities of the projectile were measured during the impact tests using a high-speed digital camera Photron FastCam SA-Z.

The residual velocity obtained for each impact velocity is resumed in Fig. 14. The results shown have been fitted via the expression proposed by Recht and Ipson [36] as follows:

$$V_r = a\cdot(V_0^{\kappa} - V_{bl}^{\kappa})^{1/\kappa} \quad (4)$$

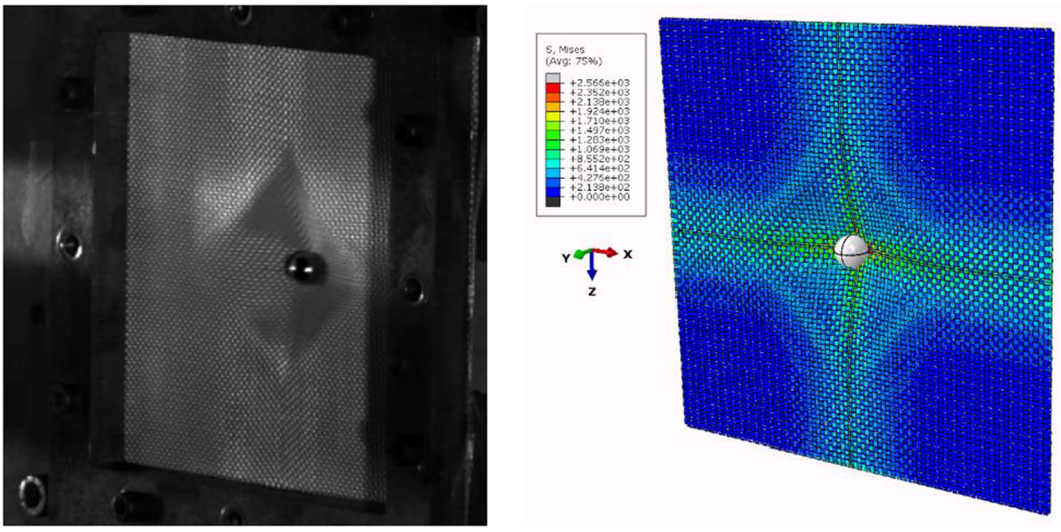

Fig. 17. Comparison between experimental and numerical ballistic impact test at a certain instant.

where a and κ are empirical constants which best fit the data and V_{bl} is the ballistic limit. The original Recht-Ipson model indicates that $a = m_p/(m_p - m_{pl})$ and $\kappa = 2$, where m_p and m_{pl} denote the mass of the projectile and plug, respectively, and is applicable only if the plastic deformation of the projectile is negligible. Observations of experimental data from the literature show that the penetration process of 7.62 mm APM2 projectile does not involve any significant plugging. Therefore, a was set as 1 and κ was fitted to the data trend line. The method of least squares was used to obtain the best fit for κ and V_{bl} [37]. In this work, these parameters have been determined as determined as $\kappa = 2.31$ for fabric A and $\kappa = 2.05$ for fabric B.

In view of the results, it can be seen how the ballistic limit for fabric A is smaller than for fabric B. It should be noted that the friction coefficients of fabric A are almost 1.85 times the friction coefficients of fabric B and, in addition, the areal density is slightly higher (1.034 times) than that of fabric A. Therefore, it is reasonable to think that the influence of friction on the ballistic limit is very important, as it has been analysed by Ha-Minh et al. [6], where ballistic impact simulations are made against fabrics establishing four scenarios: considering friction between yarns and also between yarns and projectile, considering friction only between yarns, considering friction only between projectile and yarns and not considering friction in any case. As a conclusion of that work it was verified that the friction component that most influences the results of a ballistic impact is the one existing between yarns, followed by the friction between them and projectile. This conclusion was revealed by Rao [20], who found that friction between yarns is clearly more important than the friction between the projectile and the fabric.

It is necessary to be careful while carrying out the ballistic analysis using the absorbed energy density (E_v) of yarn since it involves fill and warp direction yarns. According to the results obtained in Section 3.1, the E_v for fabric A is higher in warp direction and lower in fill direction than for fabric B.

4.2. Numerical model

This section describes the numerical Finite Element Model developed to apply all the mechanical properties obtained in the previous sections (elastic Modulus, failure stress, failure strain and inter-yarn friction coefficient). The model has been developed using the commercial code ABAQUS/Explicit. The modelling of the fabric has been made at the mesoscopic level, modelling the fill and the warp as three-dimensional solids to shape the final fabric in a way as realistic as possible. Only a quarter of the model has been developed applying symmetry conditions in both directions and clamping the outside edges, Fig. 15.

Both static and kinetic inter-yarn friction coefficients have been introduced in the model using the values obtained experimentally in Section 3.2 and using the following static-kinetic exponential decay law:

$$\mu = \mu_k + (\mu_S - \mu_k)e^{-\alpha \cdot |V_{rel}|} \tag{5}$$

where V_{rel} is the relative velocity between the respective surfaces in contact and α is an exponential decay coefficient, characteristic of the transition from static to dynamic friction of the contacting entities.

The model is capable of accurately reproducing the impact-velocity curves obtained experimentally, as shown in Fig. 16a and b for fabrics A and B respectively. Regarding to the value of ballistic limit, the differences between the experimental and numerical results are presented in Table 6, along with the values of the numerical fitting parameters, κ, obtained from Eq. (4). In all cases, the error is below 12%, therefore the model can be validated and used to analyze the influence of different parameters.

In Fig. 17, a comparison between experimental test and numerical model of the ballistic impact process of fabrics A is presented as an example, to check the reproducibility of the results after applying the results obtained in Sections 2 and 3.

5. Conclusions

In this study, a complete characterization of different para-aramid fabrics at fill and warp directions was carried out in quasi-static conditions. Several experimental tests have been carried out: yarn uniaxial tensile tests, yarn pull out tests and fabric uniaxial tensile tests. Once the characterization of the fabrics was carried out, a numerical impact model was developed and validated with experimental results.

The experimental and numerical results obtained in this paper both for soft and hard fabrics, could be synthesized as:

- The mechanical properties of fill-yarns are greater than warp-yarns.
- The maximum pull-out force increases with the number of transverse threads that the yarn pulled out must cross, being this force higher in warp than in fill direction.
- The friction coefficients increase with the width of the yarn due to the greater contact surface denoted by the angle θ.

- Large differences have been found in fabric tensile tests. The fabric with less thickness and more fibers per m^2 showed a greater crimp region.
- The fabric with the highest coefficient of friction also had the highest absorbed energy density.
- The unidirectional aramid fibre cross-plied at 0°/90° hard fabric, is the material which absorb a great amount of energy density, even more that the soft fabrics.
- In general, the reinforced aramid woven fabrics absorb less energy density than soft fabrics.
- In the analysis carried out against the impact of steel spherical projectiles, the fabric with the highest energy absorbed per unit volume and friction coefficient presented the best ballistic performance.

This study provides the basis for a deeper analysis of aramid fabrics against ballistic threats and sharp threats. It is important to highlight that these results can be used in the development of impact numerical models, such as the one proposed in this work, which allow the prediction of the ballistic limit and ballistic curve with great precision.

Acknowledgement

The authors acknowledge the financial support for the work to the Ministry of Economy and Competitiveness of Spain under the Project RTC-2015-3887-8 and DPI2017-88166-R for the financial support of the work.

References

[1] Dong Z, Sun CT. Testing and modeling of yarn pull-out in plain woven Kevlar fabrics. Compos Part A Appl Sci Manuf 2009;40:1863–9. https://doi.org/10.1016/j.compositesa.2009.04.019.
[2] Zhu D, Soranakom C, Mobasher B, Rajan SD. Experimental study and modeling of single yarn pull-out behavior of kevlar® 49 fabric. Compos Part A Appl Sci Manuf 2011;42:868–79. https://doi.org/10.1016/J.COMPOSITESA.2011.03.017.
[3] Godfrey TA, Rossettos JN. The onset of tear propagation at slits in stressed uncoated plain weave fabrics. J Appl Mech 1999;66:926–33.
[4] Tapie E, Shim VPW, Guo YB. Influence of weaving on the mechanical response of aramid yarns subjected to high-speed loading. Int J Impact Eng 2015;80:1–12. https://doi.org/10.1016/J.IJIMPENG.2014.12.010.
[5] Nilakantan G, Gillespie JW. Yarn pull-out behavior of plain woven Kevlar fabrics: effect of yarn sizing, pullout rate, and fabric pre-tension. Compos Struct 2013;101:215–24. https://doi.org/10.1016/J.COMPSTRUCT.2013.02.018.
[6] Ha-Minh C, Boussu F, Kanit T, Crépin D, Imad A. Effect of frictions on the ballistic performance of a 3D warp interlock fabric: numerical analysis. Appl Compos Mater 2012;19:333–47. https://doi.org/10.1007/s10443-011-9202-2.
[7] Valizadeh M, Ravandi SAH, Salimi M, Sheikhzadeh M. Determination of internal mechanical characteristics of woven fabrics using the force-balance analysis of yarn pullout test. J Text Inst 2008;99:47–55. https://doi.org/10.1080/00405000701567712.
[8] Bilisik K, Korkmaz M. Single and multiple yarn pull-outs on aramid woven fabric structures. Text Res J 2011;81:847–64. https://doi.org/10.1177/0040517510391703.
[9] Shockey D, Erlich D, Simons J. Improved barriers to turbine engine fragments: interim report II. SRI Int 1999. DOT/FAA/AR.
[10] Bilisik K, Korkmaz M. Multilayered and multidirectionally-stitched aramid woven fabric structures: experimental characterization of ballistic performance by considering the yarn pull-out test. Text Res J 2010;80:1697–720. https://doi.org/10.1177/0040517510365954.
[11] Gawandi A, Thostenson ET, Gilllespie JW. Tow pullout behavior of polymer-coated Kevlar fabric. J Mater Sci 2011;46:77–89. https://doi.org/10.1007/s10853-010-4819-3.
[12] Bai R, Li W, Lei Z, Ma Y, Qin F, Fang Q, et al. Experimental study of yarn friction slip and fabric shear deformation in yarn pull-out test. Compos Part A Appl Sci Manuf 2018;107:529–35. https://doi.org/10.1016/j.compositesa.2018.02.001.
[13] Das S, Jagan S, Shaw A, Pal A. Determination of inter-yarn friction and its effect on ballistic response of para-aramid woven fabric under low velocity impact. Compos Struct 2015;120:129–40. https://doi.org/10.1016/J.COMPSTRUCT.2014.09.063.
[14] Kirkwood KM, Kirkwood JE, Lee YS, Egres Jr. RG, Wagner NJ, Wetzel Eric D. Yarn pull-out as a mechanism for dissipating ballistic impact energy in kevlar® KM-2 fabric part i: quasi-static characterization of yarn pull-out. Text Res J 2004;74:920–8.
[15] Kirkwood JE, Kirkwood KM, Lee YS, Egres RG, Wagner NJ, Wetzel ED. Yarn pull-out as a mechanism for dissipating ballistic impact energy in kevlar® KM-2 fabric part ii: predicting ballistic performance. Text Res J 2004;74:939–48. https://doi.org/10.1177/004051750407401101.
[16] Martínez MA, Navarro C, Cortés R, Rodríguez J, Sanchez-Galvez N. Friction and wear behaviour of Kevlar fabrics. J Mater Sci 1993;28:1305–11. https://doi.org/10.1007/BF01191969.
[17] Pan N, Yoon M-Y. Behavior of yarn pullout from woven fabrics: theoretical and experimental. Text Res J 1993;63:629–37. https://doi.org/10.1177/004051759306301103.
[18] Bazhenov S. Dissipation of energy by bulletproof aramid fabric. J Mater Sci 1997;32:4167–73. https://doi.org/10.1007/BF02806188.
[19] Sadegh AM, Cavallaro PV. Mechanics of energy absorbability in plain-woven fabrics: an analytical approach. J Eng Fiber Fabr 2012;7:10–25.
[20] Rao MP, Duan Y, Keefe M, Powers BM, Bogetti TA. Modeling the effects of yarn material properties and friction on the ballistic impact of a plain-weave fabric. Compos Struct 2009;89:556–66. https://doi.org/10.1016/J.COMPSTRUCT.2008.11.012.
[21] Seretis GV, Kostazos PK, Manolakos DE, Provatidis CG. On the mechanical response of woven para-aramid protection fabrics. Compos Part B Eng 2015;79:67–73. https://doi.org/10.1016/j.compositesb.2015.04.025.
[22] Beex LAA, Verberne CW, Peerlings RHJ. Experimental identification of a lattice model for woven fabrics: application to electronic textile. Compos Part A Appl Sci Manuf 2013;48:82–92. https://doi.org/10.1016/J.COMPOSITESA.2012.12.014.
[23] Duan Y, Keefe M, Bogetti TA, Cheeseman BA. Modeling the role of friction during ballistic impact of a high-strength plain-weave fabric. Compos Struct 2005;68:331–7. https://doi.org/10.1016/J.COMPSTRUCT.2004.03.026.
[24] Nilakantan G, Keefe M, Wetzel ED, Bogetti TA, Gillespie JW. Computational modeling of the probabilistic impact response of flexible fabrics. Compos Struct 2011;93:3163–74. https://doi.org/10.1016/J.COMPSTRUCT.2011.06.013.
[25] Nilakantan G, Gillespie JW. Ballistic impact modeling of woven fabrics considering yarn strength, friction, projectile impact location, and fabric boundary condition effects. Compos Struct 2012;94:3624–34. https://doi.org/10.1016/J.COMPSTRUCT.2012.05.030.
[26] Nilakantan G, Wetzel ED, Bogetti TA, Gillespie JW. Finite element analysis of projectile size and shape effects on the probabilistic penetration response of high strength fabrics. Compos Struct 2012;94:1846–54. https://doi.org/10.1016/J.COMPSTRUCT.2011.12.028.
[27] Nilakantan G, Wetzel ED, Bogetti TA, Gillespie JW. A deterministic finite element analysis of the effects of projectile characteristics on the impact response of fully clamped flexible woven fabrics. Compos Struct 2013;95:191–201. https://doi.org/10.1016/J.COMPSTRUCT.2012.07.023.
[28] Nilakantan G, Nutt S. Effects of fabric target shape and size on the V50 ballistic impact response of soft body armor. Compos Struct 2014;116:661–9. https://doi.org/10.1016/J.COMPSTRUCT.2014.06.002.
[29] British Standards Institution.: 2009. Textiles – Yarns from packages – Determination of single-end breaking force and elongation at break using constant rate of extension 2009:15. doi: ISO 2062:2009.
[30] Briscoe BJ, Motamedi F. The ballistic impact characteristics of aramid fabrics: the influence of interface friction. Wear 1992;158:229–47. https://doi.org/10.1016/0043-1648(92)90041-6.
[31] Tan VBC, Zeng XS, Shim VPW. Characterization and constitutive modeling of aramid fibers at high strain rates. Int J Impact Eng 2008;35:1303–13. https://doi.org/10.1016/J.IJIMPENG.2007.07.010.
[32] British Standards Institution. Textiles – Tensile properties of fabrics. Part 1: determination of maximum force and elongation at maximum force using the strip method. Bs Iso 13934-1 1999:18. doi: 10.1007/s00401-002-0622-9.
[33] Potop GLLAL. The influence of weft density and weave on the weaving shrinkage in narrow fabrics. Bul AGIR 2016;3:95–8.
[34] Bilisik K, Erdogan G, Sapanci E. In-plane response of para-aramid/phenolic nanostitched and nanoprepreg 3D composites under tensile loading. Polym Compos 2018:1–12. https://doi.org/10.1002/pc.24847.
[35] Parsons EM, Weerasooriya T, Sarva S, Socrate S. Impact of woven fabric: experiments and mesostructure-based continuum-level simulations. J Mech Phys Solids 2010;58:1995–2021. https://doi.org/10.1016/j.jmps.2010.05.006.
[36] Recht RF, Ipson TW. Ballistic perforation dynamics. J Appl Mech 1963;30:384–90. https://doi.org/10.1115/1.3636566.
[37] Rahman NA, Abdullah S, Zamri WFH, Abdullah MF, Omar MZ, Sajuri Z. Ballistic limit of high-strength steel and Al7075-T6 multi-layered plates under 7.62-mm armour piercing projectile impact. Lat Am J Solids Struct 2016;13:1658–76. https://doi.org/10.1590/1679-78252657.